



Steady-state spectroscopy and ultrafast dynamics of flavylum derivatives in the red spectral region

Ahmed H. Ismail^a, M. Faisal Khyasudeen^{a,b}, John Husband^a, A. Ramadan Ibrahim^a, Younis Baqi^a, Osama K. Abou-Zied^{a,*}

^a Department of Chemistry, Faculty of Science, Sultan Qaboos University, P.O. Box 36, Postal Code 123, Muscat, Sultanate of Oman

^b Centre for Fundamental and Frontier Sciences in Nanostructure Self-Assembly, Department of Chemistry, Faculty of Science, University of Malaya, 50603, Kuala Lumpur, Malaysia

ARTICLE INFO

Keywords:

Flavylum
Red spectral region
Absorption
Fluorescence
Ultrafast dynamics

ABSTRACT

In an effort to enhance the absorption and fluorescence of flavylum in the red spectral region, we synthesized a 2'-hydroxyflavylum derivative (FLV-OH) with a rigid electron donating julolidine group attached to position 7 and examined its ground and excited states spectroscopy by absorption, fluorescence, ultrafast dynamics, and by density functional theory (DFT). The precursor compound without the hydroxyl group (FLV) was also synthesized and characterized in order to clarify the role of the intramolecular hydrogen bond on the spectroscopy of FLV-OH. The absorption and fluorescence spectra of both compounds indicate the stability of the flavylum ion in methanol and in aqueous acidic and neutral solutions. The $S_1 \leftarrow S_0$ absorption peaks at 540 nm and extends to 620 nm, whereas the corresponding fluorescence has two peaks and extends to 900 nm. The ability of the flavylum moiety to undergo ring opening to form chalcone is observed in basic solution. The presence of the hydroxyl group in FLV-OH promotes the formation of a quinonoidal base which was not possible in FLV. DFT and time-dependent (TD)-DFT calculations point to the existence of only one species within the lowest energy band in the absorption and fluorescence spectra. Femtosecond fluorescence upconversion and transient absorption measurements reveal the solvation dynamics within the initial 1–2 ps after photoexcitation, followed by molecular relaxation to the ground state. The latter was measured to be 505 ps in FLV-OH and 164 ps in FLV. The longer lifetime of FLV-OH in the excited state is correlated to the presence of a hydrogen bond (OH...O) that tends to stabilize the excited molecule. This H-bond was estimated from TD-DFT to be 1.83 Å in the S_1 state which is shorter than that in S_0 (1.91 Å). The stability of the excited state of FLV-OH was also reflected in the measured fluorescence quantum yield of 0.038, compared to 0.016 for FLV, in addition to its large molar absorptivity ($\epsilon_{540} = 52,500 \text{ M}^{-1} \text{ cm}^{-1}$ for FLV-OH vs $12,500 \text{ M}^{-1} \text{ cm}^{-1}$ for FLV). The current results indicate that FLV-OH has spectroscopic properties that make it suitable for many applications such as a potential light harvesting dye in solar cells.

1. Introduction

The search for new compounds that can absorb and fluoresce in the red and near-infrared (NIR) spectral window is receiving increasing attention from scientists due to the importance of such compounds in many chemical, physical and biological applications. Among such applications are dye-sensitized solar cells and biological imaging. Energy harvesting at the photon-rich NIR end of the solar spectrum is expected to boost solar-to-electrical conversion efficiency. On the other hand, the optical window 600–1000 nm offers imaging at significant depths in

living tissues [1,2].

Flavylum compounds belong to a class of naturally occurring water-soluble anthocyanins that are responsible for the red and purple colors of many flowers and fruits [3]. Their complex chemistry derives mainly from the different forms that can be stabilized by changing the pH of the solution. The flavylum cation (Fig. 1) is the stable form at low pH. In order to stabilize the flavylum cation over a wide range of pH, electron donating groups were attached to position 7 of the molecule [4–7]. For example, 7-(*N,N*-diethylamino)-4'-hydroxyflavylum has a pK_a of 6.6 [7], whereas replacing the diethylamine group by a rigid julolidine

* Corresponding author.

E-mail address: abouzied@squ.edu.om (O.K. Abou-Zied).

<https://doi.org/10.1016/j.jlumin.2020.117261>

Received 13 February 2020; Received in revised form 27 March 2020; Accepted 30 March 2020

Available online 4 April 2020

0022-2313/© 2020 Elsevier B.V. All rights reserved.

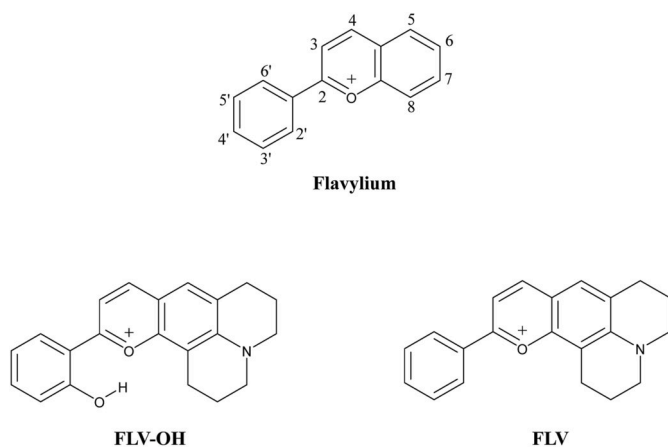


Fig. 1. Structures of flavylium, FLV-OH and FLV.

group (2,3,6,7-tetrahydro-1*H*,5*H*-benzo[*ij*]quinolizine) extends the pK_a to 7.5 due to the increased electron donating ability of the N-atom [4]. However, due to the presence of the OH group in the 4'-position, the cation loses a proton and converts to a quinonoidal form as the pH is raised toward neutrality which triggers a ring opening to form chalcone. Although the presence of a rigid group is expected to enhance the fluorescence quantum yield, Avó et al. recently showed that twisted intramolecular charge transfer in the open diethylamino substituent has no influence on the quantum yield of fluorescence which was measured to be lower by 2.5 times in the rigid julolidine derivative [4].

To this end, we synthesized a new flavylium derivative that has the OH group attached in position 2' (FLV-OH, Fig. 1). We introduced a julolidine group in the molecular structure, with the N-atom attached to position 7. The high electron donating ability of this amino group [8,9] and its rigidity play an essential role in shifting the absorption and fluorescence spectra to less energy. In order to clarify the role of the presence of the OH group in the 2'-position, we also synthesized the precursor compound with no OH group (FLV in Fig. 1). In FLV, the formation of the quinonoidal form is not structurally possible. We compare in this work the steady-state absorption and fluorescence behaviour of the two compounds (FLV-OH and FLV) in MeOH and in different pH aqueous solutions. Density functional theory (DFT) was used in order to predict the molecular geometry in the ground and excited states, and to simulate the steady-state spectra. We extended the study to include femtosecond time-resolved measurements in order to shed light on the effect of the intramolecular hydrogen bond in FLV-OH in stabilizing the excited state and increasing the fluorescence quantum yield.

2. Experimental

2.1. Synthesis of FLV-OH and FLV

2.1.1. Materials and methods

All starting materials and solvents were purchased from commercial suppliers and were used as received. Thin-layer chromatography was performed using TLC aluminium sheets silica gel 60 F₂₅₄. Synthesized compounds were visualized under UV light (254 nm). ¹H and ¹³C NMR data were collected on Bruker Avance 500 MHz (¹H) or 126 MHz (¹³C), respectively. DMSO-*d*₆ and methanol-*d*₄ were used as solvents. Chemical shifts are reported in parts per million (ppm) relative to the deuterated solvents (DMSO-*d*₆), δ ¹H: 2.49 ppm, ¹³C: 39.7 ppm and (methanol-*d*₄), δ ¹H: 3.31 and 4.87 ppm, ¹³C: 49.1 ppm. Coupling constants *J* are given in Hertz and spin multiplicities are given as *s* (singlet), *d* (doublet), *t* (triplet), *q* (quartet), *p* (pentet), *m* (multiplet), *br* (broad). Mass spectra were collected by HPLC-(UV)-ESI-MS using the same procedure as previously described [10]. Melting points were determined on an electro

thermal capillary apparatus and are uncorrected. Lyophilization was performed using freeze dryer type Alpha 1–4 LSCplus.

2.1.2. Chemistry

The flavylium compounds (FLV and FLV-OH) were synthesized by a newly developed synthetic protocol (Scheme 1). Thionyl chloride (SOCl₂) was employed for the condensation reaction of an equimolar concentration (1 mmol) between 8-hydroxyjulolidine-9-carboxaldehyde (IUPAC: 2,3,6,7-tetrahydro-8-hydroxy-1*H*,5*H*-benzo[*ij*]quinolizine-9-carboxaldehyde) and acetophenone or its derivative (2'-hydroxyacetophenone) furnishing chalcone intermediates, which are readily insito and undergo an intermolecular cyclization reaction followed by the loss of a water molecule to produce the target compounds (FLV-OH and FLV) in high isolated yields (70–75%), see Scheme 1. In brief, the two reactants were dissolved in absolute ethanol (10 mL) and the resulting mixture was kept under stirring at room temperature, followed by portion-wise addition of four equivalent of SOCl₂. The reaction mixture was monitored by TLC using methanol/DCM (5%) as eluent and the reaction was complete in 2–6 days. Solvents were evaporated using rotary evaporator, and the resulting materials were dissolved in water (100 mL) and extracted with dichloromethane (3 × 100 mL). The aqueous layer was lyophilized using a freeze-dryer, to obtain dark blue powder.

2.1.3. Spectral data of the synthesized FLV-OH and FLV

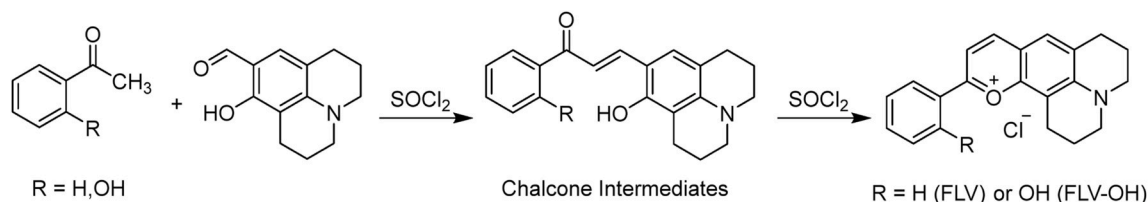
FLV: m.p. 128–130°C. ¹H NMR (DMSO-*d*₆) δ 1.949, (q, *J* = 5.0, 4.5 Hz, 2H, CH₂), 2.012 (q, *J* = 5.0, 4.5 Hz, 2H, CH₂), 2.888 (t, *J* = 5.5, 5.0 Hz, 2H, CH₂-Ar), 3.028 (t, *J* = 5.5, 5.0 Hz, 2H, CH₂-Ar), 3.620 (bdd, *J* = 4.0, 3.0 Hz, 4H, 2CH₂-N), 7.709–7.650 (m, 4H-aromatic), 8.000 (d, *J* = 6.5 Hz, 1H-aromatic), 8.230 (d, *J* = 6.0 Hz, 1H-aromatic), 8.570 (d, *J* = 6.5 Hz, 1H-aromatic). ¹³C NMR (DMSO-*d*₆) δ 19.11, 19.37 (2 CH₂), 20.16, 27.46 (2 CH₂-Ar), 50.96, 51.40 (2 CH₂-N), 105.16, 108.59, 120.56, 127.60, 127.89, 129.79, 130.14, 130.57, 133.77, 146.26, 153.46, 153.91, & 163.43 (C-aromatics), LC-MS (*m/z*): 301.9 [M – H]⁺

FLV-OH: m.p. 240°C (decomposed). ¹H NMR (methanol-*d*₄) δ 2.101 (q, *J* = 5.5, 5.0 Hz, 2H, CH₂), 2.171 (q, *J* = 5.5, 5.0 Hz, 2H, CH₂), 2.997 (t, *J* = 5.0, 4.5 Hz, 2H, CH₂-Ar), 3.140 (t, *J* = 5.0, 4.5 Hz, 2H, CH₂-Ar), 3.685 (dd, *J* = 5.0, 4.0 Hz, 4H, 2CH₂-N), 7.126 (dd, *J* = 16.7, 7.8 Hz, 2H-aromatic), 7.537–7.508 (m, 1H-aromatic), 7.546 (s, 1H-aromatic), 8.120 (dd, *J* = 6.5, 1.0 Hz, 1H-aromatic), 8.217 (d, *J* = 6.5 Hz, 1H-aromatic), 8.412 (d, *J* = 7.0 Hz, 1H-aromatic). ¹³C NMR (methanol-*d*₄) δ 18.92, 19.19 (2 CH₂), 19.96, 27.26 (2 CH₂-Ar), 50.52, 50.96 (2 CH₂-N), 104.84, 111.78, 116.77, 117.05, 119.50, 120.24, 127.11, 128.51, 129.28, 134.51, 145.72, 153.15, 154.31, 158.37, & 163.01 (C-aromatics), LC-MS (*m/z*): 336.38 [M + NH₄⁺]⁺, 317.38 [M – H][–]

2.2. Steady-state spectroscopic measurements

For spectroscopic measurements in different pH aqueous solutions, a universal buffer was used which is composed of 0.1 M each of citric acid, potassium phosphate, sodium tetraborate, Tris, and potassium chloride [11]. The pH was adjusted by adding aliquots of aqueous 1.0 M NaOH. Deionized water (Millipore) was used in the preparations. The concentration of FLV-OH and FLV in MeOH and buffer solutions was 0.02 mM for all the experiments.

Absorption spectra were obtained with an HP 845x Diode Array spectrophotometer. Fluorescence spectra were recorded on a Duetta spectrofluorometer (Horiba Scientific). Fluorescence quantum yield of FLV-OH and FLV in methanol (MeOH) was estimated using DCM dye ([2-[2-[4-(dimethylamino)phenyl]ethenyl]-6-methyl-4H-pyran-4-ylidene]-propanedinitrile) in MeOH as the reference (fluorescence quantum yield, ϕ_F = 0.437 [12]), and the software (FluorTools.com) was used for data analysis. In all the experiments, samples were contained in a 1 cm path length quartz cell and the measurements were conducted at 23 ± 1 °C.



Scheme 1. Synthesis of the flavylum compounds (FLV-OH and FLV).

2.3. Time-resolved spectroscopic measurements

2.3.1. Femtosecond transient-absorption spectroscopy

The ultrafast transient absorption measurements were performed using a femtosecond laser setup that was previously described in detail [13,14]. Briefly, pump and probe pulses were obtained using a regenerative amplified Ti:Sapphire laser (Libra, Coherent). The Libra generates compressed laser pulses (70 fs pulse width) with output of 4.26 W at a repetition rate of 5 kHz and centered at 800 nm. The output beam was split into two parts. The major portion of the output pulse was used to pump a Coherent OPerA Solo (Light Conversion Ltd.) optical parametric amplifier to generate spectrally tunable light spanning the range 240–2600 nm and is used as the pump beam. The remaining small portion of the laser output was focused on a sapphire crystal to generate a white light continuum in the range 430–800 nm which is used as the probe beam in a Helios transient absorption spectrometer (Ultrafast Systems, LLC). The probe light was measured by a fiber optic that is coupled to a multichannel spectrometer with a CMOS sensor in the range 350–850 nm. Chirp in the white light continuum probe was minimized by using parabolic mirrors. Rotational contribution to the overall excited state decay kinetics was removed by depolarizing the pump beam using a depolarizer (DPU-25, Thorlabs). The pump pulse was attenuated to ~150–200 nJ in order to avoid multiphoton excitation.

The pump and probe pulses were focused on the sample and the temporal delay of the probe pulse was varied using a computer-controlled optical delay stage (up to 5 ns with a shortest delay step of 20 fs). Kinetic traces at appropriate wavelengths were assembled from the time-resolved spectral data. Surface Xplorer software (supplied by Ultrafast Systems) was used for data analysis. The instrument response function (IRF) was measured from Raman scattering to be ~120 fs.

2.3.2. Femtosecond fluorescence-upconversion spectroscopy

A Halcyone fluorescence upconversion setup (Ultrafast Systems, LLC) was used to measure the femtosecond fluorescence dynamics. The femtosecond laser system, employed in the transient absorption setup, was used by removing two movable mirrors in order to direct the pump and probe (gate) beams to the Halcyone box (Ultrafast Systems). The gate pulse was delayed over a maximum of 5 ns in a shortest step size of 20 fs with a computer-controlled optical delay stage. The pump pulse was focused onto the sample and fluorescence was collected and focused by a parabolic mirror on a 0.5 mm BBO type II crystal. For frequency upconversion, the gate pulse (800 nm) was overlapped with the fluorescence signal in the BBO crystal, and focused slightly behind the crystal (~10 mm). The upconversion signal was focused on the entrance slit of a double monochromator and measured by a PMT detector with a spectral range of 200–800 nm. A depolarizer (DPU-25, Thorlabs) was used in the pump beam (attenuated to ~150–200 nJ) in order to remove any rotational contribution to the overall excited state decay kinetics. For the current experiment, the upconversion signal at 359 nm (sum-frequency generation) was detected which is the production of mixing fluorescence at 650 nm with the gate pulse at 800 nm. The IRF under the current non-collinear geometry was determined to be 400–500 fs from the upconversion signal of Raman scattering from water. Surface Xplorer software was used for data analysis.

The samples were prepared for the transient absorption and

fluorescence upconversion experiments in 2 mm fused silica cuvettes (Spectrocell Inc.) and were stirred during the experiment to avoid photodegradation.

3. Results and discussion

3.1. Steady-state spectra and DFT calculations

The absorption and fluorescence spectra of FLV-OH and FLV dissolved in MeOH are shown in Fig. 2. There is a large similarity in the absorption spectra of the two compounds, whereas the fluorescence spectra show a small red shift in FLV (8–12 nm). Table 1 summarizes the spectroscopic parameters. The presence of OH causes a large increase in the molar extinction coefficient of FLV-OH ($\epsilon_{540} = 52,500 \text{ M}^{-1} \text{ cm}^{-1}$ for FLV-OH vs $12,500 \text{ M}^{-1} \text{ cm}^{-1}$ for FLV). Both molecules show structured absorption and fluorescence spectra, with two major fluorescence peaks. The absorption spectra show multi peaks that extend to the red (600–620 nm), compared to some of the chalcone precursors [4–6, 14–16]. Excitation at any wavelength within the spectral region of the lowest energy absorption peak (450–580 nm) yields the same fluorescence band shown in Fig. 2. The measured fluorescence quantum yield (ϕ_F) of FLV-OH is more than double that of FLV (Table 1), indicating more excited state stability in the former due to the presence of the OH group and its ability to form an internal hydrogen bond with the benzyropyrylium oxygen.

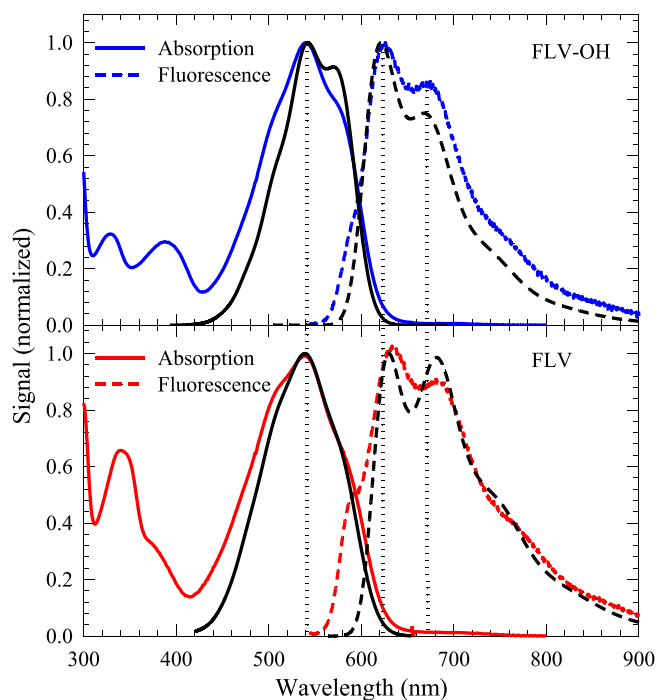


Fig. 2. Absorption and fluorescence ($\lambda_{\text{ex}} = 540 \text{ nm}$) spectra of FLV-OH and FLV dissolved in MeOH. Black lines show the calculated, (TD-DFT) vibrational-resolved spectra.

Table 1
Spectroscopic parameters for FLV-OH and FLV dissolved in MeOH.

| | $\lambda_{\max, \text{Abs}}$ (nm) | $\lambda_{\max, \text{Fluor}}^a$ (nm) | ϵ ($\lambda_{\max, \text{Abs}}$) ($\text{M}^{-1} \cdot \text{cm}^{-1}$) | ϕ_F | τ_1 (ps) ^b | $\alpha_1^{b,c}$ | τ_2 (ps) ^b | $\alpha_2^{b,c}$ |
|--------|-----------------------------------|---------------------------------------|--|----------|----------------------------|------------------|----------------------------|------------------|
| FLV-OH | 540 | 627, 675 | 52,500 | 0.038 | 1.63 ± 0.26 | 0.37 | 505 ± 29 | 0.63 |
| FLV | 540 | 635, 687 | 12,500 | 0.016 | 1.57 ± 0.24 | 0.46 | 164 ± 17 | 0.54 |

^a Excitation was at 540 nm.

^b Measured by fluorescence upconversion. $\lambda_{\text{ex}} = 575$ nm and $\lambda_{\text{detection}} = 650$ nm.

^c Contribution from the total decay transient.

The ground-state structures of FLV-OH and FLV were calculated using the DFT-B3LYP method with a 6–311++G(2d,p) basis set as implemented in Gaussian 09 [17]. Gas-phase and polarizable continuum model (PCM) calculations were performed. The structures were fully optimized without any symmetry constraint and the nature of the stationary points was confirmed with frequency calculations. Cartesian coordinates for the optimized geometries are given in the Supplementary Information (SI, Table S1). The optimized geometries reveal the twist of the phenyl and benzopyrylium moieties with respect to each other at a dihedral angle of approximately 20–25° in FLV-OH and 15° in FLV (SI, Fig. S1). The larger angle in FLV-OH can be attributed to the steric hindrance between the phenyl-OH and one of the julolidine hydrogens at small dihedral angles. Even with the twisted geometry, an internal H-bond is clearly observed with an OH...O⁺ bond distance of 1.91 Å (PCM). A benzopyrylium to nitrogen bond-length of approximately 1.35 Å, and the trigonal-planar geometry of the nitrogen atom indicate considerable double bond character for the benzopyrylium-nitrogen bond. A relatively short carbon-carbon bond (1.45–1.46 Å) is also noted for the phenyl to benzopyrylium linkage. The results are summarized in Table 2 and in SI. According to the results for the ground state, the resonance structures in Scheme 2 may be established with a large contribution from structure 2 where a hydrogen bond (OH...O) is stabilized in FLV-OH.

Time dependent (TD) calculations, employed at the same DFT method as for the ground state, were used to investigate the excited state. Calculations were performed at the optimized ground-state geometry (vertical excitation) and at the optimized geometry for the lowest excited singlet state (S_1). Findings are summarized in Table 2 and cartesian coordinates for the optimized geometries are given in Table S2, SI. The shortening of the phenyl to benzopyrylium bond length and

Table 2
Summary of DFT and TD-DFT calculations for FLV-OH and FLV^a.

| | FLV-OH | | FLV | |
|--------------------------------------|-----------|--------|-----------|--------|
| | Gas phase | PCM | Gas phase | PCM |
| Ground state (S_0) | | | | |
| ϕ (°) | 19.7 | 24.8 | 14.6 | 14.9 |
| r_{C-C} (Å) | 1.447 | 1.456 | 1.461 | 1.461 |
| r_{C-N} (Å) | 1.350 | 1.347 | 1.346 | 1.347 |
| μ (D) | 3.75 | 6.32 | 2.18 | 3.70 |
| O (natural charge) | −0.498 | −0.492 | −0.458 | −0.457 |
| N (natural charge) | −0.421 | −0.414 | −0.419 | −0.413 |
| $\Delta E_{\text{(LUMO-HOMO)}}$ (eV) | 2.789 | 2.825 | 2.886 | 2.819 |
| Excited state (S_1) | | | | |
| ϕ (°) | 8.6 | 12.5 | 1.0 | 0.3 |
| r_{C-C} (Å) | 1.417 | 1.425 | 1.422 | 1.427 |
| r_{C-N} (Å) | 1.371 | 1.360 | 1.369 | 1.360 |
| μ (D) | 3.12 | 8.32 | 5.16 | 8.16 |
| O (natural charge) | −0.532 | −0.525 | −0.458 | −0.466 |
| N (natural charge) | −0.382 | −0.342 | −0.354 | −0.329 |
| $\lambda_{\text{absorption}}$ (nm) | 487 | 493 | 489 | 490 |
| $\lambda_{\text{emission}}$ (nm) | 606 | 625 | 622 | 634 |

ϕ : Phenyl to benzopyrylium dihedral angle.

r_{C-C} : Phenyl to benzopyrylium bond length.

r_{C-N} : Benzopyrylium to nitrogen bond length.

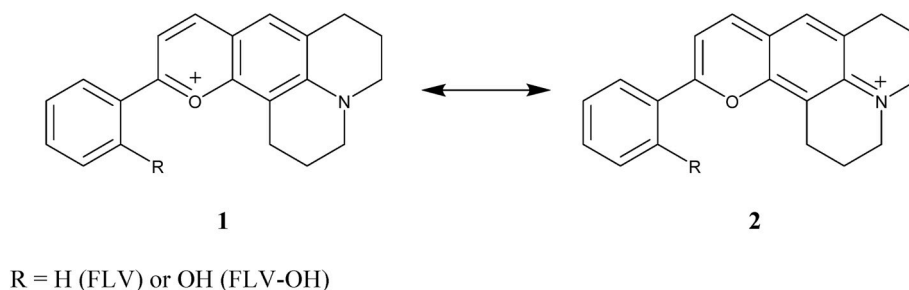
^a For S_1 , the dipole moments and atomic charges are quoted at the optimized ground-state geometry (vertical excitation).

reduction in the dihedral angle; the lengthening of the benzopyrylium to nitrogen bond; the less negative nitrogen atomic charge (calculated from the natural population analysis) and the concurrent increase in negative charge at the oxygen; are all consistent with a transition in which electron density is moved from the benzopyrylium moiety towards the phenyl group upon excitation. This is consistent with the large ability of the amino group to donate the lone pair of electrons due to its rigid structure, compared to non-rigid structures such as 7-(*N,N*-diethylamino)-4'-hydroxyflavylium [4,7]. The increase in the negative charge on oxygen is expected to add more stability to the OH...O hydrogen bond in the excited state which is reflected in the shortening of the hydrogen bond in the S_1 state (1.83 Å, PCM). Partial atomic charges in the ground and excited states are shown in Fig. S2, SI. Pertinent molecular orbitals and an isosurface plot showing the electron difference density are included in Fig. S3, SI. The HOMO to LUMO contribution to the $S_1 \leftarrow S_0$ transition is calculated to be 99.1%, and the high degree of spatial overlap between these orbitals suggests that the S_1 state is better classified as a locally excited state rather than a charge-transfer state [18].

Excitation energies between the S_0 and S_1 states at the optimized ground ($\lambda_{\text{absorption}}$) and excited ($\lambda_{\text{emission}}$) state geometries are included in Table 2. To allow comparison between the TD-DFT calculations and the observed absorption and fluorescence spectra, the calculated vibrational frequencies in the ground and first excited states are employed to calculate the vibrationally-resolved spectra [19] as implemented in Gaussian 09. Overlaid simulated and observed spectra are shown in Fig. 2. To highlight the similarities in line shape, the simulated spectra have been shifted to better align with the observed spectra: a constant red shift of 40 nm has been applied in the case of the absorption spectra, and red shifts of 20 nm (FLV-OH) and 30 nm (FLV) were applied to the simulated emission spectra. To match the observed line widths, the predicted spectra are convoluted with a Gaussian distribution of half-width at half-maximum of 600 cm^{-1} for the absorption spectra and 500 cm^{-1} for the emission spectra. Otherwise the simulations are performed using Gaussian 09 defaults for this type of calculation. The similarities between the simulated and observed spectra in the region investigated strongly suggest that the observed peak structure can be largely attributed to $S_1 \leftrightarrow S_0$ vibrational structure from a single molecular species (FLV-OH and FLV).

As a multistate system, flavylium cation exists in equilibrium with other species and dominates only at very low pH in aqueous medium [7]. In order to detect other species, pH-dependent measurements are usually carried out [4,5,7]. We measured the absorption and fluorescence spectra of FLV-OH and FLV in aqueous solutions of pH 2.0, 7.0 and 12.0. The measurements were collected 30 min after preparation. The results are displayed in Fig. 3 (absorption) and Fig. 4 (fluorescence). As shown in the absorption spectra at pH 2.0, both FLV-OH and FLV show similar absorbance in the S_1 state spectral region. At such acidic pH, only flavylium ion dominates in both molecules. At neutral pH, a slight increase in the shoulder at ~590 nm is clearly shown in FLV-OH. According to the results of a series of titration experiments on the flavylium ion where the OH group is attached to the 4'-position [4] (see Fig. 1 for numbered positions), this shoulder is due to the stability of the quinonoidal base. Scheme 3 shows the structure of the quinonoidal base which can only be formed in FLV-OH, not possible in FLV, confirming the assignment of the shoulder at 590 nm in Fig. 3 to the quinonoidal base.

In aqueous pH 12.0, the absorption spectra show dramatic changes in



Scheme 2. Resonance structures.

which only one major peak appears at 470 nm in FLV-OH and 510 nm in FLV. In basic solution, the flavylium ion undergoes a ring-opening mechanism to form the *trans*-chalcone (*t*-CH) molecule [4,5,16,20]. The mechanism for the formation of chalcone is shown in Scheme 4. In order to confirm this assignment, we carried out DFT calculations for the chalcone precursors and the vertical transitions from the optimized structures in the ground state are displayed as vertical lines in Fig. 3 for *t*-CH-OH and *t*-CH. As shown in the same figure, a small absorption at 590 nm is still observed in FLV-OH, indicating the presence of some of the quinonoidal base.

The corresponding fluorescence spectra are shown in Fig. 4 in different pH aqueous solutions. Comparing the spectra in pH 12.0 with those in neutral and acidic solutions, it is clear that the flavylium moiety induces emission in the red to NIR region, with stability in a wide range of pH.

In order to confirm the identity of the detected species in MeOH, we acidified the solution to reach pH 1.0 (by adding one drop of HCl) and measured the absorption and fluorescence spectra. The results (Fig. S5, SI) match those of FLV-OH and FLV in neat MeOH, confirming the assignment of the flavylium moiety to be the only stable form in MeOH. The acidified solutions and the solutions in neat MeOH were kept for four days and the measurements were repeated several times during this period and no change was observed.

3.2. Excited-state ultrafast dynamics

To understand the difference between the spectroscopic behavior of FLV-OH and FLV in their excited state, the two systems were subjected to femtosecond pulses and the dynamics were measured using fluorescence upconversion and transient absorption techniques. We start with the upconversion results. Fig. 5 displays the fluorescence decay transients of FLV-OH and FLV along with the best-fit functions for detection at 650 nm, after excitation at 575 nm. The transients were measured in the time frame of the molecular decay up to 2 ns. The inset profiles show the dynamics during the initial 3 ps after excitation. A prompt increase in intensity within the instrument response represents the direct formation of the excited state from the ground state species.

The decay transients were best fitted to a biexponential function with the time constants shown in Table 1. Excitation at 450 nm (the blue side of the absorption peak, Fig. 2) produces similar dynamics, indicating the existence of only one molecular species in the excited state as confirmed by the calculations. In both systems, one short decay component (τ_1), 1.63 ps (FLV-OH) and 1.57 ps (FLV), is assigned to the average solvation time of the molecules [21,22]. During this time, the equilibrium structure of the solvent molecules (MeOH) around the excited solute is attained. This solvent response reflects a diffusive solvation process that takes place in the outer solvation shell and seems to be independent of

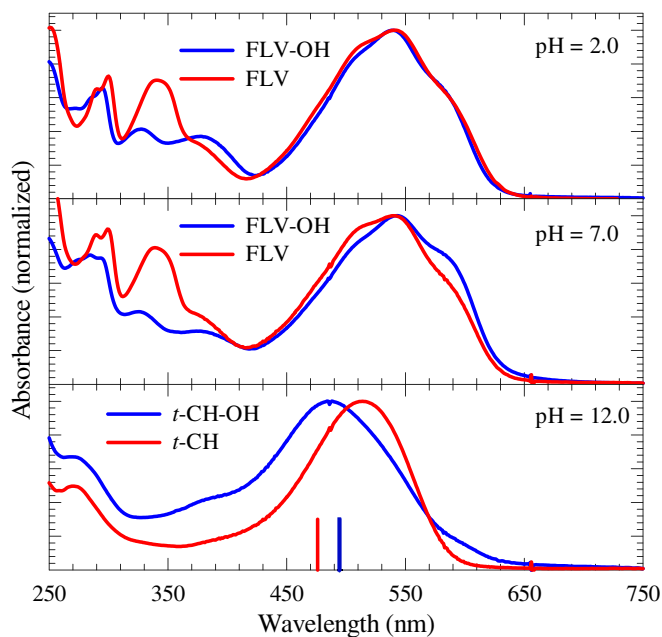


Fig. 3. Absorption spectra of FLV-OH, FLV and their corresponding *t*-CH-OH and *t*-CH in aqueous solutions of different pH. The spectra are normalized for ease of comparison. The measured spectra (not normalized) are included in Fig. S4, SI. Vertical lines represent the vertical transitions (PCM) from the optimized structures of *t*-CH-OH and *t*-CH in the ground state.

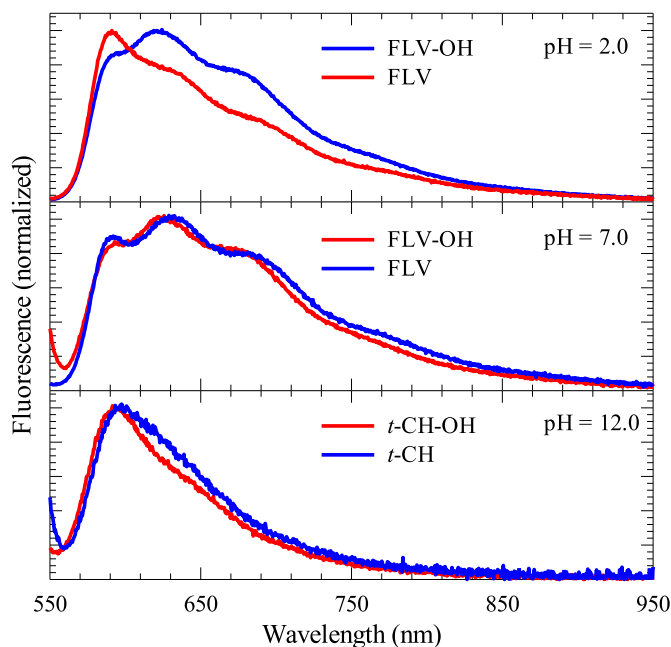
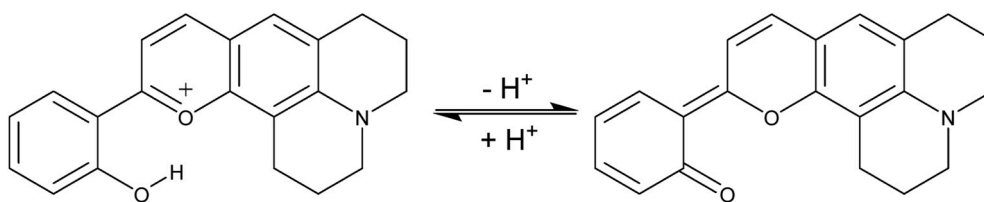
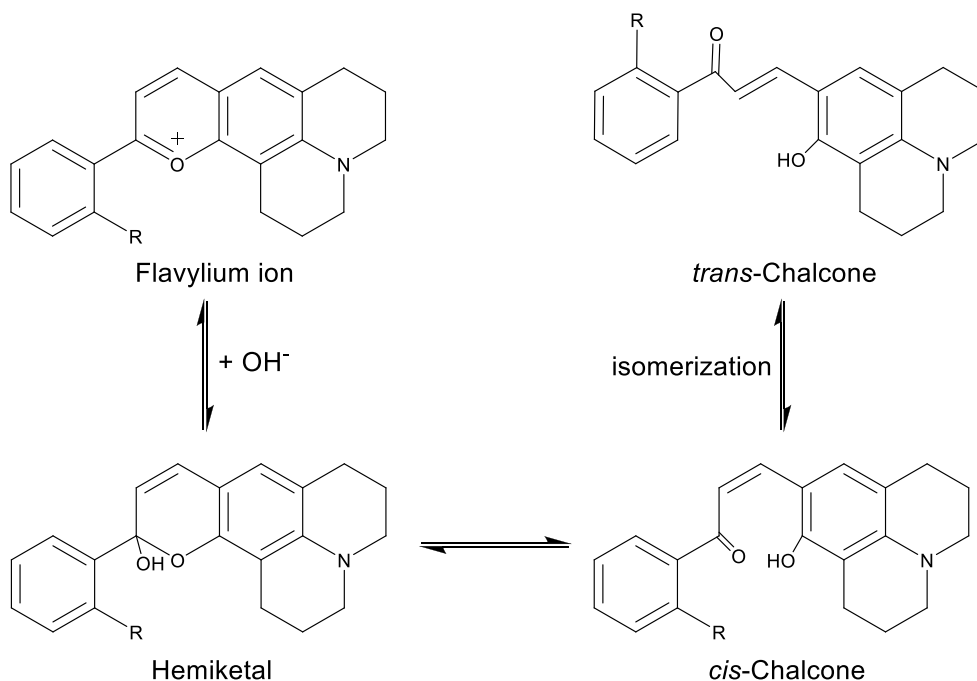


Fig. 4. Fluorescence spectra of FLV-OH, FLV and their corresponding *t*-CH-OH and *t*-CH in aqueous solutions of different pH. $\lambda_{\text{ex}} = 540$ nm.



Scheme 3. Formation of quinonoidal base by losing H^+ from FLV-OH in neutral pH aqueous solution.



Scheme 4. Equilibrium structures in acidic and neutral pH (flavylium ion) and in basic pH to form *trans*-chalcone via ring opening and isomerization.

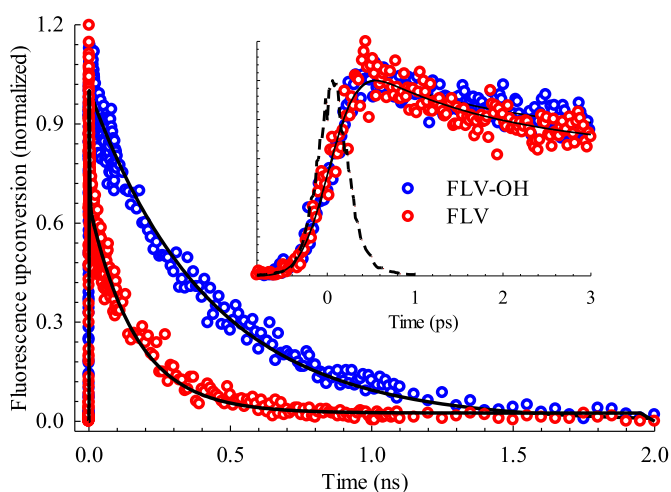


Fig. 5. Fluorescence upconversion transients of FLV-OH and FLV dissolved in MeOH. Solid lines represent the best biexponential fits. IRF is shown in dashed line. Excitation was at 575 nm and detection was for the upconverted signal ($\lambda_{\text{detection}} = 359 \text{ nm}$), corresponding to fluorescence at 650 nm. The inset shows an expanded window of the first 3 ps after excitation.

the presence of the OH group. Solvation dynamics is usually reflected in a red spectral shift during the ultrafast solvation time which can be measured as a decay component when detection is at the blue edge of the

peak and as a rise time when detection is at the red edge. For the current measurements, our detection was fixed at 650 nm (blue edge). Attempts to measure the upconverted signal that corresponds to the red edge deemed difficult due to a large amount of scattered light from the gate pulse (800 nm). We investigated the dynamics at the red edge of the spectrum using transient absorption as will be discussed below. The second decay component (τ_2) was measured to be 505 ps in FLV-OH and 164 ps in FLV, and represents the molecular relaxation to the ground state. The increase in the excited state lifetime of FLV-OH by \sim three times, compared to that of FLV, can be correlated to the presence of the intramolecular H-bond which is predicted by TD-DFT calculations to be stronger in the S_1 state (shorter OH...O distance), compared to that in the ground state. Solute-solvent electron transfer is ruled out in the current systems because of the absence of any dynamics in the sub-picosecond time scale [22]. The absence of a build up time after excitation excludes any possibility of intramolecular proton transfer or solvent-assisted proton transfer in the excited state to form a new tautomer [14,23]. This is consistent with the steady-state fluorescence spectrum of FLV-OH in MeOH in which the measured fluorescence peak is within a normal Stokes shift from the absorption spectrum (Fig. 2). This is also confirmed from the results of FLV which show similar Stokes shift.

Femtosecond transient absorption (TA) spectroscopic measurements on FLV-OH and FLV dissolved in MeOH were carried out using pump pulses of 450 and 575 nm. Both excitation energies produce similar dynamics, however the pump pulse at 575 nm is spectrally located in the middle of the TA band, causing some distortion. We show here our results for excitation at 450 nm. Fig. 6 displays snapshots of the spectral

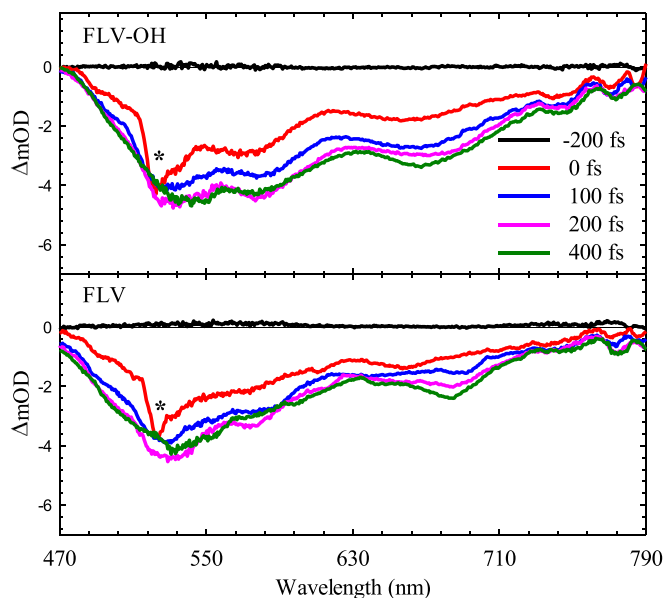


Fig. 6. Transient absorption spectra of FLV-OH and FLV dissolved in MeOH, showing the spectral change during the initial 400 fs immediately after time zero between the pump (photoexcitation at 450 nm) and the probe pulses. *: Raman scattering from the solvent.

change recorded over the initial period of 400 fs after time zero between the pump ($\lambda_{\text{ex}} = 450$ nm) and the probe. The results show a negative band that develops in the region 470–790 nm. This region covers the spectral range of the flavylum moiety in the absorption and fluorescence steady-state spectra shown in Fig. 2. The TA band can then be assigned to both ground-state bleach (GB) and stimulated emission (SE). One advantage of TA spectroscopy is the ability to probe the dynamics in the red/NIR region without much interference from the gate pulse (800 nm). For the current systems, we measured the dynamics across the SE band (600–770 nm) and the results are shown in Fig. 7. A decay component when probing at the blue side changes to a rise time component upon probing at the red side of the band. This gradual change in dynamics from decay to rise is a manifestation of solvent response. Fitting this dynamical process yields the same time constant of 1–2 ps as detected in the fluorescence upconversion results. A second

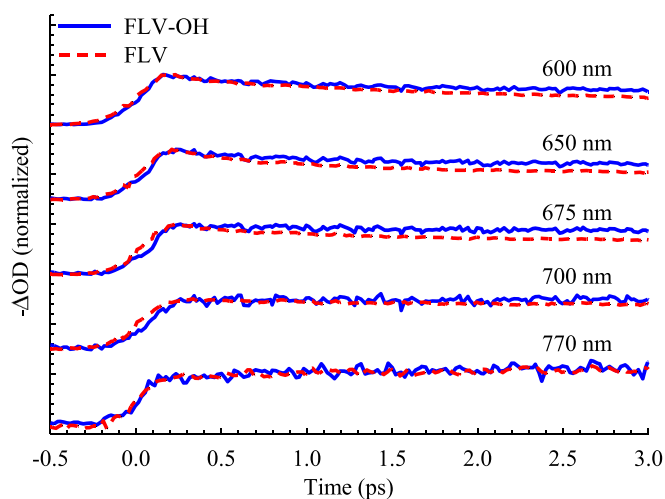


Fig. 7. Dynamics of FLV-OH and FLV dissolved in MeOH, derived from the transient absorption spectra shown in Fig. 6. The transients were monitored at different probe wavelength, as indicated.

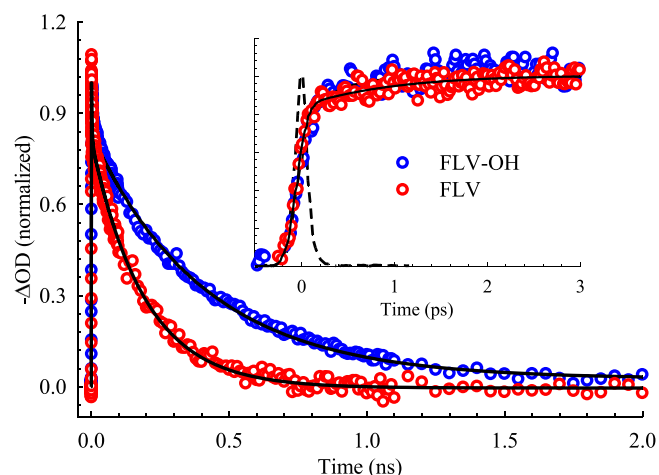


Fig. 8. Transient absorption profiles of FLV-OH and FLV dissolved in MeOH. Solid lines represent the best biexponential fits. IRF is shown in dashed line. Excitation was at 450 nm and detection was for the probe pulse at 770 nm. The inset shows an expanded window of the first 3 ps after excitation.

slower decay component in each molecule was fitted to the overall decay transients and the magnitudes of the slow decay are close to those measured by fluorescence upconversion (Table 1). Fig. 8 shows one example of the decay transients along with the biexponential fits for detection at 770 nm.

4. Conclusions

In this work, we investigated the steady-state and time-resolved spectroscopy of two flavylum derivatives (FLV-OH and FLV). The absorption and fluorescence spectra of both compounds indicate the stability of the flavylum ion in MeOH and in aqueous acidic and neutral solutions. The ability of the flavylum moiety to undergo ring opening to form chalcone is observed in basic solution. The presence of an OH group in FLV-OH promotes the formation of a quinonoidal base which was not possible in FLV. DFT and TD-DFT calculations point to the existence of only one species within the lowest energy band in the absorption and fluorescence spectra. Femtosecond fluorescence upconversion and transient absorption measurements yield two lifetime components in each molecule. One component was assigned to solvation dynamics in the excited state (1–2 ps) and the other component was assigned to molecular relaxation from the excited state to the ground state. The second component was measured to be much longer in FLV-OH (505 ps), compared to that in FLV (164 ps). The difference in the lifetime values is correlated to the presence of a hydrogen bond (OH...O) that tends to stabilize the FLV-OH compound in the excited state. The much longer lifetime in FLV-OH explains the higher fluorescence quantum yield that was measured to be 0.038 for FLV-OH vs 0.016 for FLV.

The stability of FLV-OH and FLV in a wide range of pH, their absorption in the red spectral region, and their fluorescence that extends to NIR, all point to spectroscopic properties that should be useful in many applications such as in bioimaging and as dye concentrators in solar cells. The presence of the OH group in the 2'-position shows more stability of the excited state, as evidenced in the increased fluorescence quantum yield and lifetime of FLV-OH which should be helpful in future modifications in the flavylum structure.

Declaration of competing interest

The authors declare no conflict of interest.

CRedit authorship contribution statement

Ahmed H. Ismail: Data curation. **M. Faisal Khyasudeen:** Data curation. **John Husband:** Formal analysis. **A. Ramadan Ibrahim:** Data curation. **Younis Baqi:** Methodology, Formal analysis. **Osama K. Abou-Zied:** Methodology, Supervision, Writing - original draft.

Acknowledgement

This work was supported by Sultan Qaboos University through His Majesty's Trust Fund for Strategic Research (SR/SCI/CHEM/18/01) and Omantel fund (EG/SQU-OT/19/1). Y.B. was supported by a grant from the Arab-German Young Academy of Sciences and Humanities, AGYA, (AGYA_2019_TP_50).

Appendix A. Supplementary data

Supplementary data to this article can be found online at <https://doi.org/10.1016/j.jlumin.2020.117261>.

References

- [1] M.Y. Berezin, H. Lee, W. Akers, S. Achilefu, Near infrared dyes as lifetime solvatochromic probes for micropolarity measurements of biological systems, *Biophys. J.* 93 (2007) 2892–2899.
- [2] R. Weissleder, A clearer vision for *in vivo* imaging, *Nat. Biotechnol.* 19 (2001) 316–317.
- [3] F. Pina, M.J. Melo, C.A.T. Laia, A.J. Parola, J.C. Lima, Chemistry and applications of flavylum compounds: a handful of colours, *Chem. Soc. Rev.* 41 (2012) 869e908.
- [4] J. Avó, V. Petrov, N. Basílio, A.J. Parola, F. Pina, Evidence against the twisted intramolecular charge transfer (TICT) model in 7-aminoflavylum derivatives, *Dyes Pigments* 135 (2016) 86–93.
- [5] R. Matsushima, H. Mizuno, H. Itoh, Photochromic properties of 4'-amino-substituted 2-hydroxychalcones, *J. Photochem. Photobiol., A* 89 (1995) 251–256.
- [6] R. Matsushima, M. Suzuki, Photochromic properties of 2-hydroxychalcones in solution and polymers, *Bull. Chem. Soc. Jpn.* 65 (1992) 39–45.
- [7] M.C. Moncada, D. Fernandez, J.C. Lima, A.J. Parola, C. Lodeiro, F. Folgosa, et al., Multistate properties of 7-(N,N-Diethylamino)-40-hydroxyflavylum. An example of an unidirectional reaction cycle driven by pH, *Org. Biomol. Chem.* 2 (2004) 2802–2808.
- [8] A.C. Benniston, S. Clift, A. Harriman, Intramolecular charge-transfer interactions in a julolidine–Bodipy molecular assembly as revealed via ¹³C NMR chemical shifts, *J. Mol. Struct.* 985 (2011) 346–354.
- [9] A. Nano, M.P. Gullo, B. Ventura, N. Armadori, A. Barbieri, R. Ziesel, Panchromatic luminescence from julolidine dyes exhibiting excited state intramolecular proton transfer, *Chem. Commun.* 51 (2015) 3351–3354.
- [10] Y. Baqi, C.E. Müller, Synthesis of alkyl- and aryl amino-substituted anthraquinone derivatives by microwave-assisted copper (0)-catalyzed Ullmann coupling reactions, *Nat. Protoc.* 5 (2010) 945–953.
- [11] D.D. Perrin, B. Dempsey, *Buffers for pH and Metal Ion Control*, Chapman and Hall, London, 1974.
- [12] K. Rurack, M. Spieles, Fluorescence quantum yields of a series of red and near-infrared dyes emitting at 600–1000 nm, *Anal. Chem.* 83 (2011) 1232–1242.
- [13] I. Ibrahim, H.N. Lim, O.K. Abou-Zied, N.M. Huang, P. Estrela, A. Pandikumar, Cadmium sulphide nanoparticles decorated with Au quantum dots as ultrasensitive photoelectrochemical sensor for selective detection of copper (II) ions, *J Phys Chem C* 120 (2016) 22202–22214.
- [14] N.I. Zahid, M.S. Mahmood, B. Subramanian, S.M. Said, O.K. Abou-Zied, New insight into the origin of the red/near-infrared intense fluorescence of a crystalline 2-hydroxychalcone derivative: a comprehensive picture from the excited-state femtosecond dynamics, *J. Phys. Chem. Lett.* 8 (2017) 5603–5608.
- [15] A.A. Freitas, F.H. Quina, A.A.L. Maçanita, Femtosecond and temperature-dependent picosecond dynamics of ultrafast excited-state proton transfer in water–dioxane mixtures, *J. Phys. Chem.* 118 (2014) 10448–10455.
- [16] P. Figueiredo, J.C. Lima, H. Santos, M.-C. Wigand, R. Brouillard, A.L. Maçanita, F. Pina, Photochromism of the synthetic 4',7-dihydroxyflavylum, *J. Am. Chem. Soc.* 116 (1994) 1249–1254.
- [17] M.J. Frisch, G.W. Trucks, H.B. Schlegel, G.E. Scuseria, M.A. Robb, J.R. Cheeseman, et al., *Gaussian 09*, Gaussian, Inc., Wallingford CT, 2009.
- [18] P. Zhou, J. Liu, S. Yang, J. Chen, K. Han, G. He, The invalidity of the photo-induced electron transfer mechanism for fluorescein derivatives, *Phys. Chem. Chem. Phys.* 14 (2012) 15191–15198.
- [19] V. Barone, J. Bloino, M. Biczysko, F. Santoro, Fully integrated approach to compute vibrationally resolved optical spectra: from small molecules to macrosystems, *J. Chem. Theor. Comput.* 5 (2009) 540–554.
- [20] D.A. Kalchevski, V. Petrov, A. Tadjer, A. Nenov, Impacts of hydroxylation on the photophysics of chalcones: insights into the relation between the chemical composition and the electronic structure, *Phys. Chem. Chem. Phys.* 20 (2018) 8924–8934.
- [21] M. Horng, J. Gardecki, A. Papazyan, M. Maroncelli, Subpicosecond measurements of polar solvation dynamics: coumarin 153 revisited, *J Phys Chem* 99 (1995) 17311–17337.
- [22] G.-J. Zhao, K.-L. Han, Hydrogen bonding in the electronic excited state, *Acc. Chem. Res.* 45 (2012) 404–413.
- [23] P. Zhou, K. Han, Unraveling the detailed mechanism of excited-state proton transfer, *Acc. Chem. Res.* 51 (2018) 1681–1690.